MOLECULAR ONCOLOGY 10 (2016) 966–980

available at www.sciencedirect.com

ScienceDirect

www.elsevier.com/locate/molonc

Improving fascin inhibitors to block tumor cell migration and metastasis

Shaoqin Han[a,b], *Jianyun Huang*[b], *Bingqian Liu*[b], *Bowen Xing*[b], *Francois Bordeleau*[c], *Cynthia A. Reinhart-King*[c], *Wenxin Li*[a], *J. Jillian Zhang*[b], *Xin-Yun Huang*[b,*]

[a]College of Life Sciences, Wuhan University, Wuhan, China
[b]Department of Physiology and Biophysics, Cornell University, Weill Medical College, New York, NY 10065, USA
[c]Department of Biomedical Engineering, Cornell University, Ithaca, NY 14853, USA

ARTICLE INFO

Article history:
Received 22 December 2015
Received in revised form
3 February 2016
Accepted 22 March 2016
Available online 1 April 2016

Keywords:
Metastasis
Fascin
Inhibitors

ABSTRACT

Tumor metastasis is the major cause of mortality of cancer patients, being responsible for ~90% of all cancer deaths. One of the key steps during tumor metastasis is tumor cell migration which requires actin cytoskeletal reorganization. Among the critical actin cytoskeletal protrusion structures are antenna-like filopodia. Fascin protein is the main actin-bundling protein in filopodia. Here we report the development of fascin-specific small-molecules that inhibit the interaction between fascin and actin. These inhibitors block the in vitro actin-binding and actin-bundling activities of fascin, tumor cell migration and tumor metastasis in mouse models. Mechanistically, these inhibitors likely occupy one of the actin-binding sites, reduce the binding of actin filaments, and thus lead to the inhibition of the bundling activity of fascin. At the cellular level, these inhibitors impair actin cytoskeletal reorganization. Our data indicate that target-specific anti-fascin agents will have great potential for treating metastatic tumors.

1. Introduction

Fascin is the main actin cross-linker in filopodia and shows no amino acid sequence homology with other actin-binding proteins (Adams, 2004; Bryan and Kane, 1978; Otto et al., 1979; Vignjevic et al., 2003, 2006; Yamashiro-Matsumura and Matsumura, 1985). It fastens 10–30 parallel actin filaments together into straight, compact, and rigid bundles, to form filopodia (60–200 nm in diameter) and to impart distinct mechanical stiffness to actin bundles (Claessens et al., 2006; Tilney et al., 1998; Mattila and Lappalainen, 2008). Filopodia are finger-like plasma membrane protrusions that are formed upon remodeling of the actin cytoskeleton beneath the plasma membrane (Mattila and Lappalainen, 2008). They can be viewed as a sensory organ of the cells that are used to detect and assimilate signals as well as to explore and move into the surrounding microenvironment (Bentley and Toroian-Raymond, 1986; Davenport et al., 1993; Sanders et al., 2013). They are also involved in transporting signaling proteins within tissues over a long range (Sanders et al., 2013).

Metastatic tumor cells are rich in filopodia, and the numbers of filopodia correlate with their invasiveness

* *Corresponding author*. Tel.: +1 212 746 6362.
E-mail address: xyhuang@med.cornell.edu (X.-Y. Huang).
http://dx.doi.org/10.1016/j.molonc.2016.03.006

(Coopman et al., 1998; Wang et al., 2002). Filopodium-like protrusions have also been shown to be critical for metastatic tumor cells to interact with the metastatic microenvironment and to grow at the secondary tissues (Shibue et al., 2012). Tumor metastasis is responsible for ~90% death of cancer patients. Metastasis is a multi-step process wherein a primary tumor spreads from its initial site to secondary tissues/organs (Fidler, 2003). Tumor cell migration and invasion are critical for tumor metastasis (Aznavoorian et al., 1993; Condeelis et al., 2005; Davies and Goldberg, 2011; Fornier, 2011; Partin et al., 1989; Roussos et al., 2011; Sondak et al., 2011). Migration provides tumor cells the ability to leave the primary tumor bed (local invasion), enter into blood vessels (intravasation), then exit the circulation and infiltrate the distant tissues/organs (extravasation). For cell migration and invasion to proceed, actin cytoskeleton must be reorganized by forming polymers and bundles to cause dynamic changes in cell shapes (Jaffe and Hall, 2005; Mogilner and Rubinstein, 2005).

Elevated levels of fascin have been found in many types of metastatic tumors and are correlated with clinically aggressive phenotypes, poor prognosis, and shorter survival (Hashimoto et al., 2011; Machesky and Li, 2010; Tan et al., 2013). Human fascin expression is low or absent in normal adult epithelial cells, but highly expressed in metastatic tumors (Grothey et al., 2000; Hashimoto et al., 2005). A systematic review and meta-analysis of 26 immunohistochemical studies (total ~9000 cancer patients) revealed that high fascin levels are associated with increased risk of mortality, lymph node metastasis, distant metastasis, and disease progression, and may provide a novel biomarker for early identification of aggressive and metastatic tumors (Tan et al., 2013). Furthermore, another systematic review and meta-analysis of 73 immunohistochemical studies (total ~5000 cancer patients) uncovered several biomarkers, including fascin, prognostic of overall survival (Ruys et al., 2014). Moreover, studies from 122 pancreatic cancer patients showed that higher levels of fascin correlate with poor outcome, time to recurrence and decreased overall survival (Li et al., 2014). In addition, two recent studies of fascin protein levels in circulating serum of non-small-cell lung cancer patients and healthy volunteers, or head and neck cancer patients and healthy volunteers, show that the serum fascin protein level is markedly higher in the cancer patients, particularly in advanced cases (stage III or IV), compared with that in the healthy volunteers (Lee et al., 2015; Teng et al., 2013). The serum fascin level reflects the aggressive progress of both lymphatic and distant metastasis, and is an independent prognostic factor (Teng et al., 2013). These data from human cancer patients demonstrate a correlated role for fascin in cancer progression and metastasis.

Mouse genetic studies have shown that fascin gene-knockout mice are normal, likely due to the functional compensation of other actin-bundling proteins during embryonic development (Yamakita et al., 2009). However, deletion of fascin gene delayed tumor development, slowed the tumor growth, reduced metastatic colonization, and increased overall survival in a spontaneous mouse model of pancreatic cancer (Li et al., 2014). Moreover, transgenic expression of fascin in mouse intestinal epithelium increased the tumor incidence, promoted tumor progression, and decreased the overall survival in a spontaneous mouse model of colorectal cancer (Schoumacher et al., 2014). Similarly, when ectopically expressed in tumor cells, fascin promotes tumor cell migration, invasion and metastasis (Hashimoto et al., 2011). It has also been suggested that up-regulation of fascin is part of the program of epithelial-to-mesenchymal transition (EMT) that confers motility and invasion properties on tumor cells (Machesky and Li, 2010). Therefore, fascin has been suggested as a therapeutic target for blocking tumor cell migration, invasion and metastasis (Cao et al., 2005; Chen et al., 2010; Darnel et al., 2009; Grothey et al., 2000; Hashimoto et al., 2004, 2005; Maitra et al., 2002; Pelosi et al., 2003; Rodriguez-Pinilla et al., 2006; Yoder et al., 2005; Zigeuner et al., 2006).

Previously we solved the X-ray crystal structures of the wild-type fascin and four fascin mutants to define the active and inactive configurations of fascin, and revealed the structural basis for the conformational changes of fascin during the actin-binding process (Chen et al., 2010; Yang et al., 2013). From a systematic mutagenesis study of 100 fascin mutants, we identified at least two major actin-binding sites on fascin, and that each of these actin-binding sites is essential for filopodial formation in cells (Yang et al., 2013). Impairment of any one of the individual actin-binding sites abolishes the actin-bundling activity of fascin (Yang et al., 2013). We used cryo-electron tomography and analyzed the in vitro reconstituted unconstrained three-dimensional bundles formed by fascin and actin filaments. These bundles consisted of a hexagonal lattice of parallel actin filaments where fascin formed the cross-bridges, and these bundles were similar to the filopodial bundles isolated from native tissues/cells (Yang et al., 2013). We then screened chemical libraries and identified small molecule compounds that specifically inhibit the biochemical function of fascin to bundle actin filaments (Huang et al., 2015). Here we report our optimization of one of the initial fascin inhibitor hits. The improved fascin inhibitors block the actin-binding and actin-bundling activities of fascin, breast tumor cell migration, and metastasis in mouse models. Furthermore, we reveal that these inhibitors likely occupy one of the actin-binding sites leading to the inhibition of the bundling activity of fascin. Moreover, in cellular studies, these inhibitors impair actin cytoskeletal reorganization such as filopodial formation, lamellipodial formation, stress fiber formation and focal adhesion turnover. These fascin inhibitors could be further developed for clinical uses to treat metastatic tumors.

2. Materials and methods

2.1. *Chemistry*

Compound syntheses and analyses were done by the company ValueTek Inc. (NJ, USA). All reagents and solvents were purchased from Sigma–Aldrich Chemical Co., Combi-Block Inc., Astatech Inc., Ark Pharma Inc., and Frontier Scientific Inc. and were used as received. HNMR spectra were recorded on a Bruker Fourier-400 spectrometer. Crude products were purified by silica gel chromatography. For all products, the purity was ascertained to be greater than 95% by the HPLC

method using Shimadzu 2010HPLC-UV/MS system with a C-18 reverse phase column.

2.1.1. *General procedure for* **G2**

A mixture of KOH (6.95 g, 124 mmol) in DMSO (165 mL) was stirred at room temperature for 5 min 1H-indazol-3-amine (8.25 g, 62.0 mmol) was then added in one portion. The resulting mixture was stirred at room temperature for 5 min. A solution of 4-trifluoromethylbenzyl bromide (15.6 g, 65.1 mmol) in DMSO (83 mL) was then added dropwise over 30 min. When the addition was complete, the resulting mixture was stirred at room temperature for an additional 1 h. The mixture was quenched by the addition of water (200 mL). The mixture was then extracted with CH_2Cl_2 (3 × 100 mL). The combined extracts were washed with H_2O (2 × 100 mL), brine (1 × 100 mL), then dried over $MgSO_4$, filtered and concentrated *in vacuo*. Purification by flash chromatography (Silica, 200 g, 10–100% EtOAc/Hexanes) gave 1-(trifluoromethylbenzyl)-1H-indazol-3-amine (21.79 g, 56.6 mmol, 91.3% yield) as an off-white crystalline solid. MS (ESI) *m/z*: 292 (M+H)+. To a solution of 1-(trifluoromethylbenzyl)-1H-indazol-3-amine (29.2 mg, 0.10 mmol), 4,5-dimethylfuran-2-carboxylic acid (15.4 mg, 0.11 mmol), and triethylamine (45.2 μl, 0.30 mmol) in dichloromethane (2 mL) was added 2,4,6-tripropyl-1,3,5,2,4,6-trioxatriphosphinane 2,4,6-trioxide (118.6 μl, 0.20 mmol). The resulting reaction mixture was stirred at room temp for 3 h and then the solvent was removed. The crude product was purified by preparative HPLC (sunfire 5u 100 mm column, MeOH/H_2O as solvents). 26 mg of 4,5-dimethyl-N-(1-(4-(trifluoromethyl) benzyl)-1H-indazol-3-yl)furan-2-carboxamide (Compound **G2**) was obtained as a solid. MS (ESI) *m/z*: 414 (M+H)+.

2.1.2. *Compound* **G2**

^{1}H NMR (400 MHz, chloroform-d) δ 8.73 (s, 1H), 8.09–8.30 (m, 1H), 7.50–7.59 (m, 3H), 7.35–7.43 (m, 1H), 7.24–7.33 (m, 4H), 7.17 (ddd, J = 0.88, 6.99, 8.20 Hz, 1H), 6.58 (dd, J = 1.76, 3.52 Hz, 1H), 5.54 (s, 2H). MS (ESI) calcd for C20H15F3N3O2 $(M+H)^+$ *m/z* 386.10, found 386.13.

2.1.3. *Compound* **NP-G2-011**

^{1}H NMR (400 MHz, chloroform-d) δ 8.79 (s, 1H), 8.04–8.13 (m, 2H), 7.56 (d, J = 8.14 Hz, 2H), 7.37–7.46 (m, 1H), 7.27–7.34 (m, 3H), 7.20 (ddd, J = 0.88, 6.99, 8.20 Hz, 1H), 5.55 (s, 2H), 2.86 (s, 3H). MS (ESI) calcd for C20H15F3N4OS $(M+H)^+$ *m/z* 417.09, found 417.10.

2.1.4. *Compound* **NP-G2-036**

^{1}H NMR (400 MHz, chloroform-d) δ 8.80 (br. s., 1H), 8.19 (br. s., 1H), 8.01 (d, J = 8.14 Hz, 1H), 7.54 (d, J = 7.92 Hz, 2H), 7.38–7.46 (m, 1H), 7.30 (d, J = 8.58 Hz, 1H), 7.23–7.28 (m, 2H), 7.13–7.23 (m, 1H), 5.53 (s, 2H), 2.59 (s, 3H). MS (ESI) calcd for C20H15F3N4O2 $(M+H)^+$ *m/z* 401.11, found 401.10.

2.1.5. *Compound* **NP-G2-044**

^{1}H NMR (400 MHz, chloroform-d) δ 8.05–8.16 (m, 2H), 7.54 (d, J = 8.14 Hz, 2H), 7.36–7.43 (m, 1H), 7.31 (d, J = 1.98 Hz, 1H), 7.28 (d, J = 0.66 Hz, 2H), 7.26 (s, 1H), 7.18 (ddd, J = 0.88, 6.99, 8.20 Hz, 1H), 6.60 (d, J = 1.98 Hz, 1H), 5.53 (s, 2H), 2.87 (s, 3H). MS (ESI) calcd for C21H16F3N3O2 $(M+H)^+$*m/z* 400.12, found 400.12.

2.1.6. *Compound* **NP-G2-050**

^{1}H NMR (400 MHz, chloroform-d) δ 10.57 (s, 1H), 9.37 (dd, J = 1.54, 5.06 Hz, 1H), 8.47 (dd, J = 1.76, 8.36 Hz, 1H), 8.19 (d, J = 8.36 Hz, 1H), 7.75 (dd, J = 5.06, 8.58 Hz, 1H), 7.56 (d, J = 8.14 Hz, 2H), 7.37–7.46 (m, 1H), 7.27–7.36 (m, 3H), 7.20 (dt, J = 0.77, 7.54 Hz, 1H), 5.60 (s, 2H). MS (ESI) calcd for C20H14F3N5O $(M+H)^+$ *m/z* 398.12, found 398.14.

2.2. *Mouse colony*

Female BALB/c mice (6–8 week old) were purchased from Charles River. Studies using mice were performed in compliance with the Institutional Animal Care and Use Committee of Weill Medical College of Cornell University. All mice were housed in the facility of the Research Animal Resource Center of Weill Medical College of Cornell University.

2.3. *Cell culture*

Mouse 4T1 mammary tumor cells and human MDA-MB-231 breast tumor cells were obtained from ATCC. 4T1 cells were cultured in RPMI 1640 medium supplemented with 10% FBS. MDA-MB-231 cells were cultured in DMEM supplemented with 10% FBS.

2.4. *Human fascin-1 expression and purification*

Recombinant human fascin 1 was expressed as a GST fusion protein in BL21 *Escherichia coli*. 1-liter of 2YT medium with ampicillin was inoculated overnight with 3 mL of BL21/DE3 culture transformed with pGEX4T-fascin 1 plasmid and grown at 37 °C until attenuance at 600 nm (OD_{600}) reached about 0.5. The culture was then transferred to 17 °C and induced by the addition of 0.1 mM isopropyl β-d-thiogalactoside (IPTG) for 16 h. Bacteria were harvested by centrifugation at 5000 r.p.m. for 10 min. The pellets were suspended in 30 mL of Tris/HCl (20 mM Tris/HCl pH 8.0, 150 mM NaCl) supplemented with 0.2 mM PMSF, 1 mM DTT, 1% Triton X-100 and 1 mM EDTA. After sonication, the suspension was centrifuged at 15,000 r.p.m. for 30 min to remove the cell debris. The supernatant was then incubated for 2 h with 4 mL of glutathione beads (Sigma) at 4 °C. After extensive washing with Tris/HCl (20 mM Tris/HCl pH 8.0, 150 mM NaCl), the beads were resuspended in 10 mL of thrombin cleavage buffer (20 mM Tris–HCl pH 8.0, 150 mM NaCl, 2 mM $CaCl_2$, 1 mM DTT). Fascin was released from the beads by incubation overnight with 40–100 U of thrombin at 4 °C. After centrifugation, 0.2 mM PMSF was added to the supernatant to inactivate the remnant thrombin activity. The fascin protein was further concentrated with Centricon to about 50 mg/mL.

2.5. *F-actin bundling assay*

Actin-bundling activity was measured by low-speed centrifugation assay. Monomeric rabbit G-actin was induced to polymerize at room temperature in F-actin buffer (20 mM Tris-HCl at pH 8, 1 mM ATP, 1 mM DTT, 2 mM $MgCl_2$ and 100 mM KCl). Recombinant fascin proteins (wide-type or mutant) were subsequently incubated with F-actin for 30 min at

room temperature and centrifuged for 15 min at 10,000 g in an Eppendorf 5415D tabletop centrifuge. Both supernatants and pellets were dissolved in an equivalent volume of SDS sample buffer, and the amount of fascin was determined by SDS-PAGE. We measured the intensities of fascin proteins in Coomassie-stained gels and then calculated the relative actin-bundling activity.

2.6. Boyden-chamber cell migration assay

MDA-MB-231 cells (5×10^4) suspended in 100 μl starvation medium were added to the upper chamber of an insert (6.5 mm diameter, 8 μm pore size; Becton Dickson), and the insert was placed in a 24-well plate containing 700 μl starvation medium with or without 10% FBS. When used, inhibitors were added to both the upper and the lower chambers. Migration assays were performed for 6 h and cells were fixed with 3.7% formaldehyde. Cells were stained with crystal violet staining solution, and cells on the upper side of the insert were removed with a cotton swab. Three randomly selected fields (10 objectives) on the lower side of the insert were photographed, and the migrated cells were counted. Migration was expressed as average number of migrated cells in a field.

2.7. Tumor metastasis in mice

Female BALB/c mice (6–8 week old) were purchased from Charles River. 4T1 tumor cells (1×10^6) were injected subcutaneously into the abdominal mammary gland area of mice using 0.1 mL of a single-cell suspension in PBS on Day 0. Starting on Day 7, when the tumors averaged about ~4–5 mm in diameter, G2 analogues or control solvent were given every day by intraperitoneal injection at 100 mg/kg per mouse until Day 24. On Day 25, the mice were sacrificed. This dosage regiment was well tolerated with no signs of overt toxicity. Every group included 5 mice. Numbers of metastatic 4T1 cells in lungs were determined by the clonogenic assay. In brief, lungs were removed from each mouse on Day 25, finely minced and digested in 5 mL of enzyme cocktail containing 1 × PBS and 1 mg/mL collagenase type IV for 2 h at 37 °C on a platform rocker. After incubation, samples were filtered through 70 μm nylon cell strainers and washed twice with PBS. Resulting cells were suspended, plated with a series of dilutions in 10 cm tissue culture dishes in RPMI 1640 medium containing 60 μM thioguanine for clonogenic growth. Since 4T1 tumor cells are resistant to 6-thioguanine, metastasized tumor cells formed foci after 7 days, at which time they were fixed with methanol and stained with 0.03% methylene blue for counting.

2.8. Fascin and F-actin binding assay

Actin-binding activity of fascin was measured by high-speed centrifugation assay. In high-speed centrifugation assay, monomeric rabbit G-actin (10 μM) was induced to polymerize at room temperature in F-actin buffer (20 mM Tris-HCl at pH8, 1 mM ATP, 1 mM DTT, 2 mM $MgCl_2$ and 100 mM KCl). Recombinant fascin proteins were subsequently incubated with F-actin for 60 min at room temperature and centrifuged for 30 min at 150,000 g. Both supernatants and pellets were dissolved in an equivalent volume of SDS sample buffer, and separated by SDS-PAGE.

2.9. Confocal fluorescence microscopy

Cells were seeded onto laminin-coated glass coverslips in starvation condition (no serum) for 2 h with or without inhibitors (50 μM). Cells were fixed with 3.7% formaldehyde in PBS for 10 min at room temperature, permeabilized with 0.1% Triton X-100 for 5 min, and then washed 3 times with PBS. Actin filaments were labeled with 2% Alexa 488-phalloidin. The coverslips were then mounted onto slides and imaged using Zeiss LSM510 confocal microscopy.

2.10. Fluorescence recovery after photobleaching (FRAP)

Cells were transfected using the Mirius LT1 Transfection Reagent (Mirius) following the manufacturer's instructions. 24 h after the transfection, the cells expressing GFP-FAK were seeded on fibronectin-coated (10 ug/mL in PBS, 1 h at RT) glass bottom dishes (MatTec). FRAP experiments were performed with a Zeiss 710 confocal microscope equipped with an environmental chamber, according to a protocol described before (Bordeleau et al., 2010). Photobleached regions consisted of a 2 μm wide circular region enclosing a selected focal adhesion. Fluorescence within the region was measured at low laser power before bleaching and then photobleached with 8 iterations using both the 405 and 488 nm laser lines at 100% laser power. Recovery was monitored at 488 nm at 0.5 s time intervals for 80 s. In some experiments, cells expressing GFP-FAK were pre-treated with 1 μM NP-G2-044. Fluorescence during recovery was normalized to the pre-bleach intensity and for the bleaching occurring during image acquisition, as before (Bordeleau et al., 2010). Relative recovery rates were computed with Matlab (MathWorks). The half-time for fluorescence recovery towards the asymptote was extracted from the plots after curve fitting of the data to a single exponential association algorithm.

2.11. Quantification of focal adhesion dynamics

A modified version of an adhesion dynamics assay was used to measure focal adhesion disassembly rate (Bordeleau et al., 2010). Briefly, time-lapse imaging on cells expressing GFP-FAK was performed on a Zeiss 710 confocal microscope equipped with an environmental chamber. The fluorescence of individual focal adhesion was measured as function of time in ImageJ. The assembly/disassembly dynamics of FAK-containing focal adhesions was reported in terms of normalized fluorescence intensity as function of time using Matlab. The assembly/disassembly rates were then computed from the numerical derivatives of each time dependent function. Each assembly and disassembly rate constant was calculated from measurements performed on at least 120 individual focal adhesions from 7 individual cells for each condition.

2.12. Morphodynamics analysis

Image analysis was performed with Matlab according to a previously published method with some modifications (Johnson

et al., 2015). Images were subjected to an adaptive Wiener filter (1 μm window) followed by a mean filter (3 μm window) to smoothen cell edges or a top-hat filter (1 μm ring) to extract fibrillary structures. The mean filter removes features smaller than the window size while the top-hat filter increases the contrast ratio of features smaller than the window size. The images were then automatically thresholded to obtain binary images. To obtain the lamellipodial structures from the mean filtered images, any holes inside the cell resulting from the thresholding were healed by filling them. This has the added advantage of removing any internal actin structures from the analysis. The resulting structures were then eroded to fit within the original size of the cell. To obtain the filopodia, the top-hat filtered images were further subjected to a median filter to correct for intensity variation while keeping the filopodial features. The final binary lamellipodial image was then subtracted from the filopodial image to remove any internal actin structure and retain only the outward extending filopodial components. Spatiotemporal maps were generated as described (Johnson et al., 2015). Briefly, the coordinate system of each image was transformed relative to the cell centroid along angular projections in 1° increment. To obtain the protrusion speed, the difference in overlap between each consecutive time step was calculated (yielding individual pixels values of −1 for retraction and 1 for protrusion events). The calculated pixel values along each angular direction were summed and then converted to velocity.

Overlapping spatiotemporal maps were generated by combining the filopodial structures and the mean filtered lamellipodial protrusion. Protruding structures were identified as the portion of the cell extending at a speed ≥1.25 μm/min for more than 1 min and spanning ≥8°. Filopodia were identified from the angular projection as objects having an elliptic eccentricity ≥0.7 and spanning ≤4°. This process excludes unwanted large membrane protrusions resulting from filtering errors. Since any identified filopodial components are the result of the lamellipodia mask subtraction, filopodial components do not overlap with detected protrusions. Therefore, overlapping components are defined as juxtaposed elements in the same, previous or subsequent video frame.

2.13. *Statistical analysis*

Data are expressed as mean±s.e.m. and analyzed by Student's *t* test with significance defined as $p < 0.05$.

3. Results

3.1. *Optimization of small-molecule fascin inhibitors*

We had identified small-molecule inhibitors that decreased the actin-bundling activity of fascin from screening chemical libraries (Huang et al., 2015). One of the small-molecule inhibitors is N-(1-(4-(trifluoromethyl)benzyl)-1H-indazol-3-yl) furan-2-carboxamide (named **G2**) (Figure 1A). Compound **G2** directly binds to fascin with a K_d value of 5–20 μM, and inhibited the actin-bundling activity of fascin [half-maximal inhibitory concentration (IC_{50}), 5–8 μM], but not L-plastin (another actin-bundling protein) (IC_{50} > 100 μM) (Huang et al., 2015). Compound **G2** blocked tumor cell migration and invasion (IC_{50}, 50–100 μM), and tumor metastasis in mouse models (decreased ~95% at 100 mg/kg) (Huang et al., 2015). Hence Compound **G2** is an attractive hit compound. To further explore and optimize the structure-activity-relationship of Compound **G2** for greater potency to inhibit the actin-bundling activity of fascin, we designed, synthesized, and biologically evaluated **G2** analogues and obtained improved fascin inhibitors (Figure 1 B–G). **G2** analogues were individually tested for the ability to inhibit the actin-bundling activity of fascin (Some examples are shown in Figure 1 B–I). In this assay, purified fascin proteins were incubated with purified actin proteins in the absence or presence of different concentrations of analogues. Since one fascin molecule interacts with 4–5 actin molecules in the actin-fascin bundles, we used fascin (0.25 μM) and actin (1 μM) in a 1:4 ratio. After actin polymerization and bundling by fascin, the samples were centrifuged at low-speed to collect the actin bundles. Supernatants (free fascin, free actin and un-bundled F-actin polymers) and pellets (bundled actin-fascin filaments) were separated by SDS-PAGE. Gels were then stained with Coomassie blue to visualize the fascin and actin protein levels (some examples are shown in Figure 1C and F). The fractions of fascin proteins in the pellet (over total fascin proteins) were calculated and plotted against the concentrations of the analogues (Figure 1 D and G). Some of these modified analogues were more potent than **G2**. For example, **NP-G2-044** had an IC_{50} of ~0.2 μM. We should note that, given our actin-bundling assay conditions, this IC_{50} value is close to the lower sensitivity limit of our assay. Some of the modified compounds were inactive and these compounds could be used as negative controls. For example, Compounds **NP-G2-112** and **NP-G2-113** are structurally similar to Compounds **NP-G2-044** and **NP-G2-011**, respectively, but were not active in inhibiting the activity of fascin (Figure 1H and I). These initial in vitro screenings of derivatives of Compound **G2** will assist in the future development of compounds with improved potency, specificity, and pharmacological profiles for eventual clinical applications.

3.2. *Mechanism of action of the fascin inhibitors*

We investigated the biochemical mechanism of action by which fascin inhibitors block the actin-bundling function of fascin. To determine the possible binding region of Compounds **NP-G2-011** and **NP-G2-044** on fascin, we took advantage of mutant fascin proteins that we previously generated. We and others previously solved the X-ray crystal structure of fascin (Chen et al., 2010; Jansen et al., 2011; Sedeh et al., 2010). Based on the crystal structure, we generated 100 mutations of surface-exposed residues on fascin, and determined the actin-bundling and actin-binding activity of these 100 mutants (Yang et al., 2013). The residues that were critical for actin-bundling activity were clustered in three regions and may represent different actin-binding sites on fascin (Figure 2A). The X-ray crystal structures of fascin mutants from these three regions showed that these fascin mutants have the same structure (the inactive configuration) which is slightly different from that of the active configuration of wild-type fascin (Yang et al., 2013). Thus these mutations

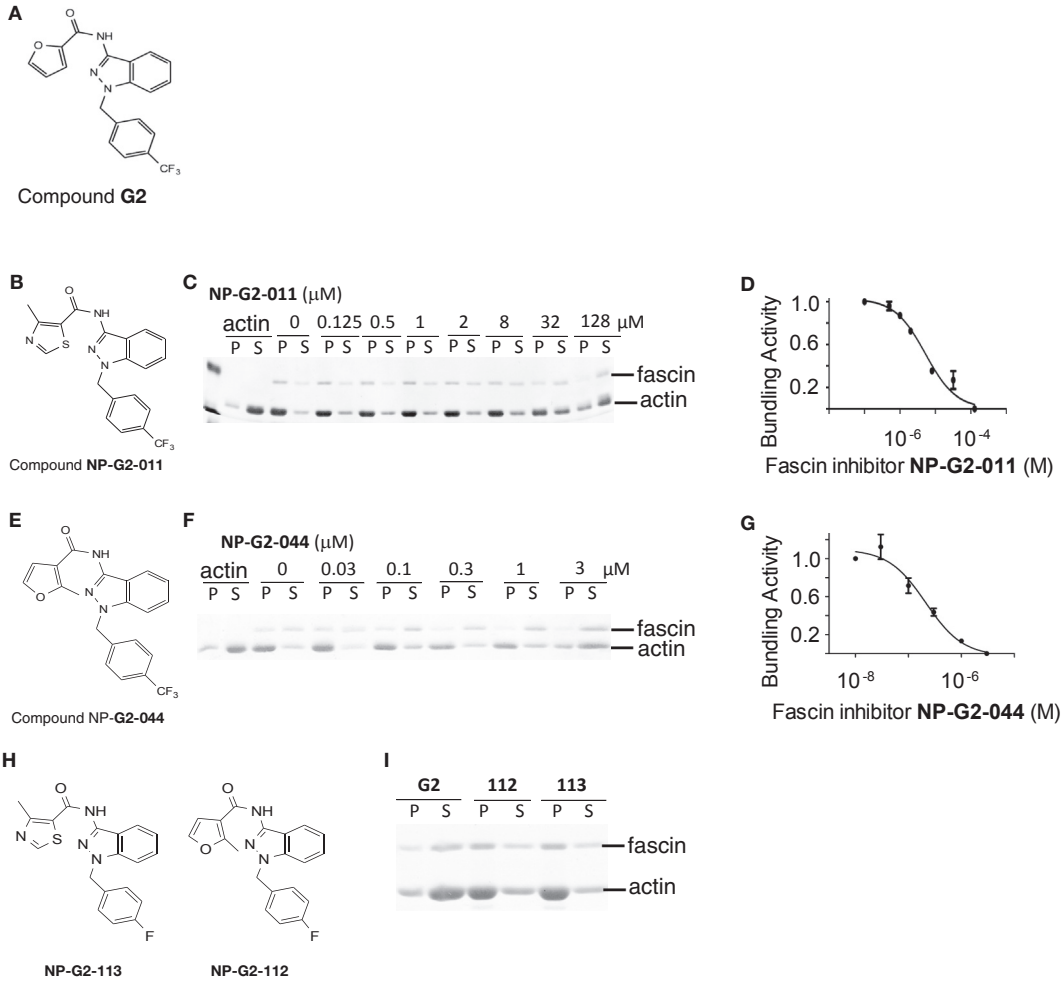

Figure 1 – Biological evaluation of analogues of Compound G2. (A) The chemical structure of Compound G2. (B) Chemical structure of Analogue NP-G2-011. (C) An example from the actin-bundling assays shows the decrease of the actin-bundling function of fascin by Compound NP-G2-011. (D) The dose response curve for Compound NP-G2-011. (E) Chemical structure of Analogue NP-G2-044. (F) An example from the actin-bundling assays shows the decrease of the actin-bundling function of fascin by Compound NP-G2-044. (G) The dose response curve for Compound NP-G2-044. (H and I) Examples of two analogues that did not show inhibitory effect on fascin. Data are representative of three similar experiments.

did not introduce major overall structural changes on fascin proteins. We have selected some of these fascin mutants and tested their sensitivity to Compounds **NP-G2-011** and **NP-G2-044**. We found that fascin (E391A) (from the actin-binding site 1) retained the actin-bundling activity but was insensitive to the inhibition by Compounds **NP-G2-011** and **NP-G2-044** (up to 400 μM) (Figure 2 B and C). Together these data demonstrate that Compounds **NP-G2-011** and **NP-G2-044** may bind to the region around residue E391. However, we should note that our previous structural data showed that the actin-binding sites on fascin are conformationally interconnected. Mutations in any one of the actin-binding sites lead to structural changes in other actin-binding sites. Hence, we could not rule out the possibility of the binding of the fascin inhibitors to other actin-binding sites.

Based on studies on enzymes, there are four types of inhibitory mechanisms: competitive inhibition, uncompetitive inhibition, non-competitive inhibition, and mixed inhibition. Although both the fascin inhibitors and actin filaments could interact with fascin, given the different structures and sizes of the fascin inhibitors and F-actin filaments, it is unlikely the fascin inhibitors use a mechanism of competitive inhibition since competitive inhibitors are often similar in structure to the real substrate. It is also unlikely an uncompetitive inhibition (in which the inhibitor binds only to the substrate–enzyme complex) as the fascin inhibitors could directly bind to fascin in the absence of F-actin filaments (Huang et al., 2015). To distinguish the mechanisms of non-competitive inhibition (in which the binding of the inhibitor does not affect the binding of substrate) versus mixed inhibition (in which the binding of the inhibitor affects the binding of the substrate), we measured the binding of actin filaments to fascin (using high-speed centrifugation assay) in the presence of the small-molecule fascin inhibitors. As shown in Figure 2 D–I, Compounds **G2**, **NP-G2-011** and **NP-G2-044** all reduced the binding between fascin and actin filaments, with similar IC_{50} values as their effects on the actin-bundling activity of fascin. With increased concentrations of

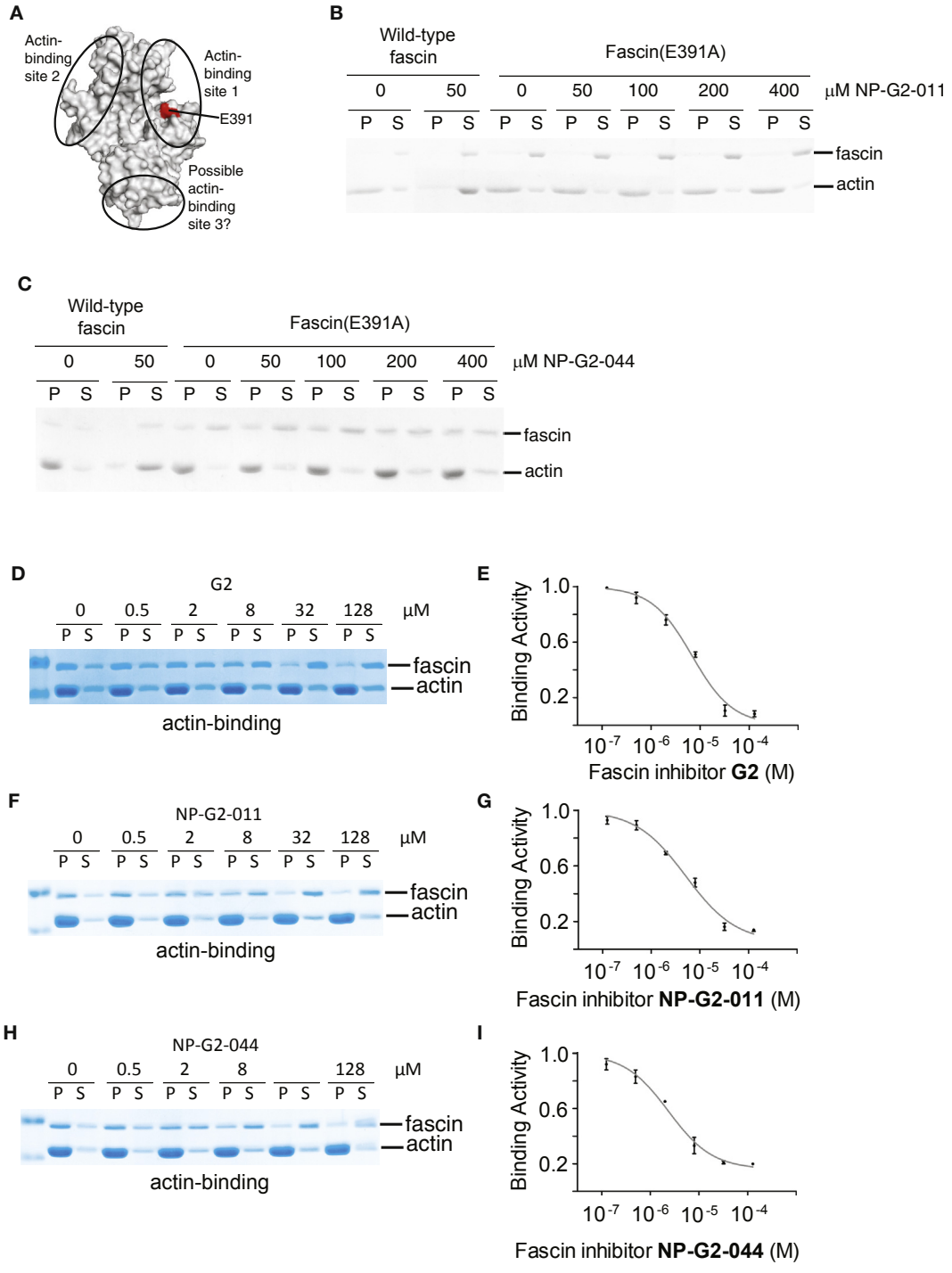

Figure 2 – Inhibitory effect of Compounds G2, NP-G2-011 and NP-G2-044 on the actin-binding activity of fascin. (A) Crystal structure of fascin shows the location of the actin-binding site 1. (B) Actin-bundling assays for wild-type fascin and fascin(E391A) in the presence of Compound NP-G2-011. (C) Actin-bundling assays with wild-type fascin and fascin(E391A) in the presence of Compound NP-G2-044. (D) An example from the actin-binding assays shows the decrease of the actin-binding function of fascin by Compound G2. (E) The dose response curve for Compound G2. (F) An example from the actin-binding assays shows the decrease of the actin-binding function of fascin by Compound NP-G2-011. (G) The dose response curve for Compound NP-G2-011. (H) An example from the actin-binding assays shows the decrease of the actin-binding function of fascin by Compound NP-G2-044. (I) The dose response curve for Compound NP-G2-044. Data are representative of three similar experiments.

inhibitors, the total amounts of actin filaments in the pellets were the same, but the amounts of bound fascin proteins were decreased (Figure 2 D, F, and H). Therefore, these data suggest these inhibitors act through mixed inhibition. These inhibitors likely change the conformation of fascin, reduce the binding of actin filaments, and thus lead to the inhibition of the bundling activity of fascin.

3.3. *Effects on actin cytoskeletal reorganization by improved fascin-specific inhibitors*

Next we explored the cellular effects of the improved fascin inhibitors on actin cytoskeletal reorganization which is critical for cell migration. Fascin is the main actin-bundling protein in filopodia. To critically evaluate that the fascin inhibitors indeed engage fascin in cells, it would be best to have a fascin mutant that does not bind to a fascin inhibitor but retains its actin-bundling activity. This mutant fascin should confer resistance to the fascin inhibitor in cells. Our above data show that fascin(E391A) is such a fascin mutant. Therefore, to investigate the specificity of these fascin inhibitors **NP-G2-011** and **NP-G2-044** in cells, we examined the filopodial formation in 4T1 breast tumor cells expressing wild-type fascin or fascin(E391A) mutant. While **NP-G2-011** and **NP-G2-044** abolished bradykinin-induced filopodial formation in 4T1 cells with wild-type fascin (Figure 3 A and C), **NP-G2-011** and **NP-G2-044** did not affect the filopodial formation in 4T1 cells re-expressing fascin(E391A) mutant (Figure 3 B and C). These data demonstrate that **NP-G2-011** and **NP-G2-044** engage the target fascin and block filopodial formation in cells, and confirm a critical role for the actin-bundling activity of fascin in filopodial formation.

Then we investigated the effect on lamellipodial formation. PDGF (platelet-derived growth factor) treatment could induce the formation of lamellipodia and membrane ruffles in a Rac-dependent manner (Jaffe and Hall, 2005). As shown in Figure 4 A and C, while PDGF induced lamellipodial formation in cells, this induction was blocked by the fascin inhibitors **NP-G2-011** and **NP-G2-044**. To ascertain these inhibitors acted via fascin to block lamellipodial formation, we used 4T1 cells expressing fascin(E391A). PDGF still induced lamellipodial formation in these cells, but the induction was insensitive to **NP-G2-044** (Figure 4, B and C). We further explored the mechanism by which fascin contributes to lamellipodial formation. Given the well-established role of fascin in filopodial formation, we tested the hypothesis that filopodia serve as templates for the formation of new lamellipodia (Johnson et al., 2015). To visualize the formation of new lamellipodia, we expressed actin-GFP in MDA-MB-231 cells. High-resolution time-lapse videos of randomly migrating cells were acquired and analyzed (Figure 4 D–H). As shown in Figure 4D, a filopodium (marked by the arrows at 0 and 30 s time points) extended and formed a lamellipodium (fan-shaped membrane protrusion at 60–150 s time points).

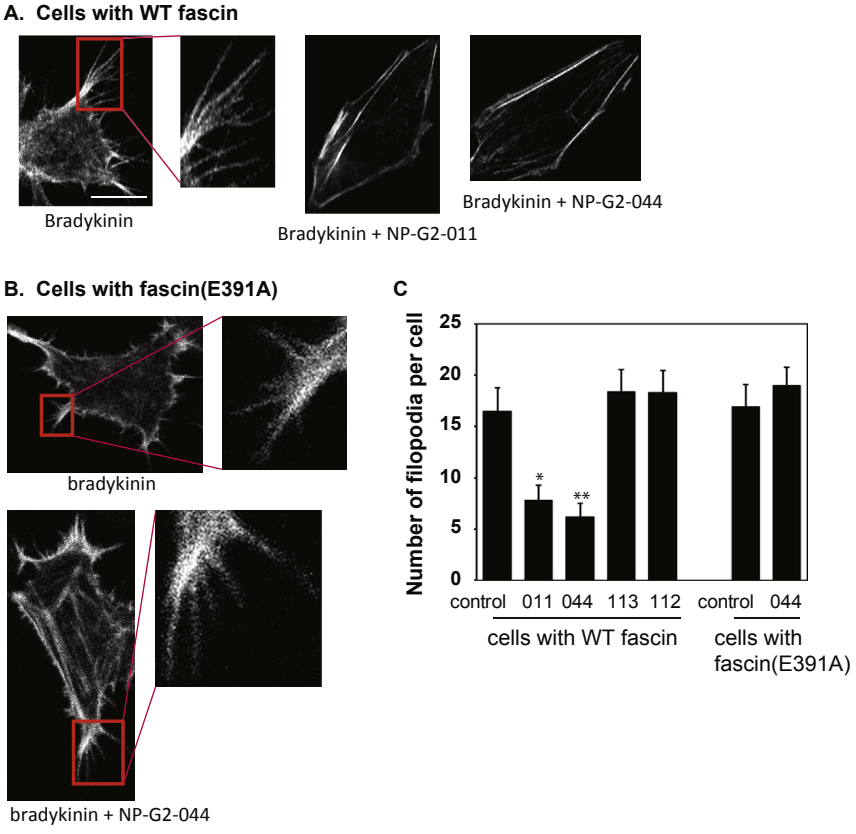

Figure 3 – Inhibitory effect of Compounds NP-G2-011 and NP-G2-044 on filopodial formation. (A) Cells with wild-type fascin were treated with bradykinin to induce filopodial formation. Addition of Compounds NP-G2-011 and NP-G2-044 blocked bradykinin-induced filopodial formation. (B) 4T1 cells expressing fascin(E391A) mutant formed filopodia upon bradykinin treatment. Filopodial formation in these cells was resistant to Compound NP-G2-044 inhibition. (C) Quantification of data in A and B. Error bars, mean±SEM. *$p < 0.01$; **$p < 0.005$. Scale bar, 10 μm.

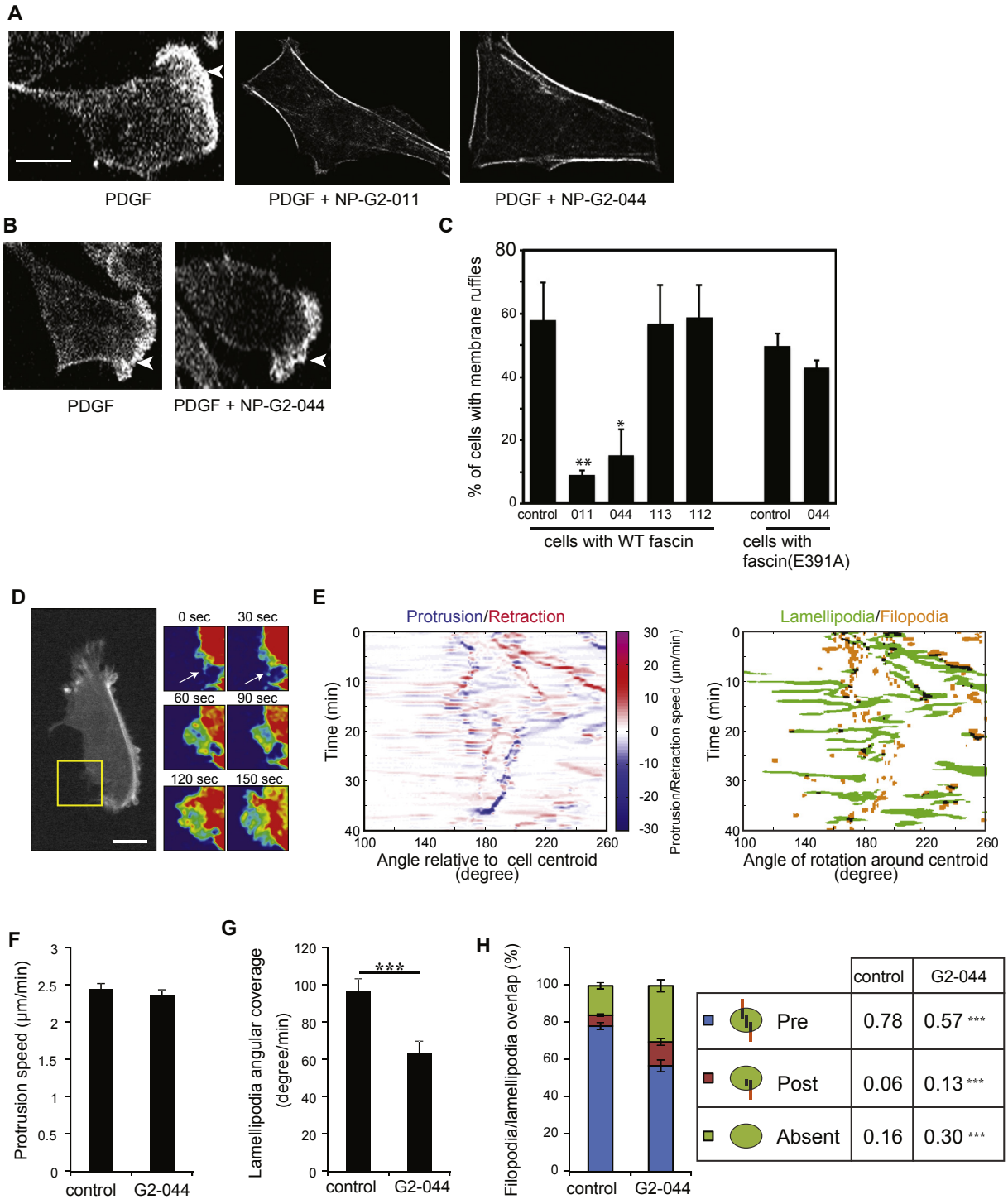

Figure 4 – Inhibitory effect of Compounds NP-G2-011 and NP-G2-044 on lamellipodial formation and the transition from filopodia to lamellipodia. (A) Cells with wild-type fascin were treated with PDGF to induce lamellipodial formation (marked by arrowheads). Addition of Compound NP-G2-011 or NP-G2-044 blocked PDGF-induced lamellipodial formation. (B) 4T1 cells expressing fascin(E391A) mutant formed lamellipodia upon PDGF treatment. Lamellipodial formation in these cells was resistant to Compound NP-G2-044 inhibition. (C) Quantification of data in A and B. Error bars, mean ± SEM. *$p < 0.05$; **$p < 0.01$. Scale bar, 10 μm. (D) Time lapse of a LifeAct-GFP expressing MDA-MB-231 cell showing a filopodium (arrow at 0 and 30 s) extending as a lamellipodium (60–150 s in zoom of yellow box sown at right). (E) Angular projection map of the protrusion and retraction speed of cell membrane extensions along with the identified lamellipodial and filopodial structure map. (F) Average protruding speed of membrane extension with and without NP-G2-044 treatment. (G) Quantification of the angular membrane fraction covered by lamellipodia with and without NP-G2-044 treatment. (H) Quantification of the lamellipodial and filopodial overlap with and without NP-G2-044 treatment. (Pre, presence of a filopodium prior to lamellipodial extension; Post, overlap of a filopodium after the extension of a lamellipodium; Absent, no overlap between filopodia and lamellipodia). Error bars, mean ± s.e.m. Scale bars, 10 μm ***$p < 0.01$.

Spatiotemporal maps of the protrusion and retraction speed of cell membrane extensions were generated (Figure 4E, left panel). These angular projection maps showed that lamellipodia coincide with protrusion over filopodia (Figure 4E, right panel). While **NP-G2-044** treatment did not affect the overall speed at which the lamellipodia were extending (Figure 4F), fascin inhibition lowered the overall angular portion of the cell contour covered by lamellipodia (Figure 4G). Furthermore, in the absence of **NP-G2-044**, 78% of the lamellipodia overlapped with pre-existing filopodia (Figure 4H). **NP-G2-044** significantly decreased the overlap of lamellipodia and filopodia (to 57%) (Figure 4H). These data demonstrate that filopodia could act as initiation hubs for new lamellipodia, and suggest that **NP-G2-044** decreases filopodial formation resulting in decreased lamellipodial formation.

Finally we investigated any possible effect on stress fiber formation and focal adhesion turnover. Stress fibers are contractile actin bundles and provide force for cell adhesion and migration. LPA (lysophosphatidic acid) could induce actin stress fiber formation through a RhoA-dependent pathway (Jaffe and Hall, 2005). While we observed the induction of actin stress fiber formation by LPA, this induction was reduced by **NP-G2-011** and **NP-G2-044** (Figure 5 A and C). On the other hand, LPA could still induce actin stress fiber formation in cells expressing fascin(E391A) even in the presence of **NP-G2-044** (Figure 5 B and C). These data demonstrate a role for fascin in actin stress fiber formation. Stress fibers are linked to the extracellular matrix via focal adhesions which are dynamic complexes. Focal adhesions allow the cell to communicate with and respond to its environment. We investigated the role of fascin in focal adhesion dynamics using our new pharmacological inhibitors of fascin. Since focal adhesion turnover has previously been shown to be related to FAK (a non-receptor tyrosine kinase) residency within focal adhesions (Bordeleau et al., 2010; Hamadi et al., 2005), we performed FRAP (fluorescence recovery after photobleaching) experiments on FAK-GFP expressing MDA-MB-231 cells. Confocal live-cell images of MDA-MB-231 cells expressing GFP-FAK were taken before photobleaching (Figure 5D). The recovery after photobleaching was recorded by time-lapse imaging (Figure 5E). The kinetics of recovery of GFP-FAK after photobleaching of focal adhesions from cells pre-treated with vehicle or **NP-G2-044** were illustrated in Figure 5F. Upon **NP-G2-044** treatment, the recovery half-life computed from the fluorescence recovery experiments decreased from 6.2 s to 3.4 s (Figure 5G), indicative of lower FAK residency and suggesting a more stable focal adhesion (Bordeleau et al., 2010; Hamadi et al., 2005). Furthermore, measurements of the focal adhesion turnover during a 40-min period using GFP-FAK expressing MDA-MB-231 cells and time-lapse confocal live-cell imaging revealed a corresponding 20–25% reduction in both the assembly and disassembly rates after fascin inhibition (Figure 5 H–L). Together, our data demonstrate a role for the actin-bundling activity of fascin in various actin cytoskeletal reorganization processes.

3.4. *Inhibition of tumor cell migration*

To test the effect of these **G2** analogues on tumor cell migration, we studied the migration of tumor cells in the absence or presence of the analogues. We used the quantitative Boyden chamber assay. MDA-MB-231 human metastatic breast tumor cells were loaded onto the top of the Boyden chamber. After about six hours, cells migrated into the bottom of the chamber filter were counted. Among the analogues, four of them had improved potency in blocking tumor cell migration comparing to Compound **G2** (Figure 6 A–F). While Compound **G2** inhibited the migration of MDA-MB-231 tumor cells with an IC_{50} of 50–100 μM, three of these analogues (**NP-G2-036**, **NP-G2-044** and **NP-G2-050**) blocked tumor cell migration with IC_{50} values of ~10 μM (Figure 6 D–F). Compound **NP-G2-112**, which did not inhibit the actin-bundling activity of fascin, did not block the migration of MDA-MB-231 cells (Figure 6G). Hence some of the analogues of Compound **G2** are with improved potency in cellular studies.

3.5. *Inhibition of tumor metastasis in mouse models*

Finally we tested the effect of Compounds **NP-G2-011** and **NP-G2-044** on tumor metastasis in animal models. In the orthotropic spontaneous tumor metastasis mouse model, 4T1 breast tumor cells were injected into the orthotropic site (the mammary gland) and then the metastasis to the lung was monitored (Chen et al., 2010; Shan et al., 2005; Yang et al., 2009) (Figure 7A). The 4T1 mouse tumor closely mimics human breast cancer in its anatomical site, immunogenicity, growth characteristics, and metastatic properties (Pulaski and Ostrand-Rosenberg, 1998). From the mammary gland, the 4T1 tumor spontaneously metastasizes to a variety of target organs including lung, bone, brain, and liver. Seven days after implantation of 4T1 tumor cells, we injected the mice with control solvent or Compound **NP-G2-011** or **NP-G2-044** (intraperitoneally and daily at 100 mg/kg). After 18 days, the mice were sacrificed and examined for metastasis in the lungs (Chen et al., 2010; Shan et al., 2005; Yang et al., 2009). Whereas mice injected with control solvent exhibited large numbers of metastasized 4T1 cells in the lungs, the number of metastasized 4T1 cells in the lungs of mice treated with Compounds **NP-G2-011** or **NP-G2-044** was reduced by ~95% (Figure 7A). We observed that Compound **NP-G2-011** or **NP-G2-044** treatment had no effect on the body weight of the mice (Figure 7B). These compounds had a minor inhibitory effect on the growth of primary tumors at later stages as measure by the volume of the primary tumors in mice (Figure 7C) and the weight of the dissected primary tumors (Figure 7D).

4. Discussion

We have obtained new fascin inhibitors with improved potency in inhibiting the actin-bundling activity and tumor cell migration. These new fascin inhibitors also decreased tumor metastasis in mouse models. We have shown that these fascin inhibitors likely act on an actin-binding site of fascin to decrease its actin-bundling activity. Using the improved fascin inhibitors, we have shown that fascin is involved in various actin cytoskeletal reorganization events such as lamellipodial formation, actin stress fiber formation, and focal adhesion turnover, in addition to filopodial formation.

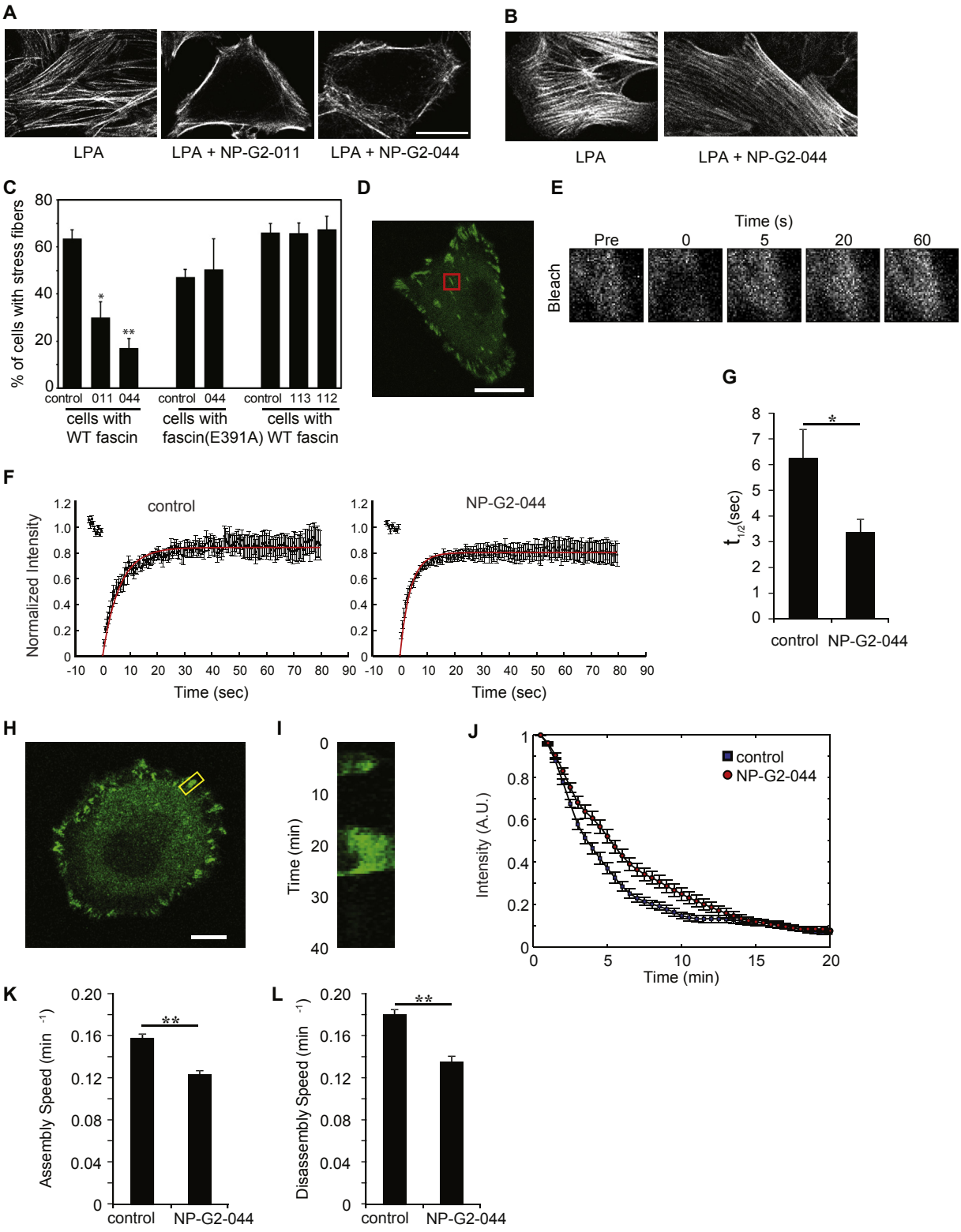

Figure 5 – Inhibitory effect of Compounds NP-G2-011 and NP-G2-044 on stress fiber formation and focal adhesion turnover. (A) Cells with wild-type fascin were treated with LPA to induce actin stress fiber formation. Addition of Compound NP-G2-011 or NP-G2-044 blocked LPA-induced stress fiber formation. (B) 4T1 cells expressing fascin(E391A) mutant formed stress fibers upon LPA treatment. Stress fiber formation in these cells was resistant to Compound NP-G2-044 inhibition. (C) Quantification of data in A and B. Error bars, mean ± SEM. *$p < 0.05$; **$p < 0.001$. Data are representative of three similar experiments. Scale bar, 10 μm. (D) Confocal live cell images of MDA-MB-231 cells expressing GFP-FAK were taken before photobleaching the ROIs (red box) containing focal adhesions. (E) Time lapse sequence of the selected ROIs showing a representative recovery after photobleaching (Pre, pre bleach). (F) Kinetics of recovery of GFP-FAK after photobleaching of focal adhesions from cells pre-treated with vehicle (Ctrl) or NP-G2-044 are illustrated. The measured fluorescence intensity was normalized and the mean values (18

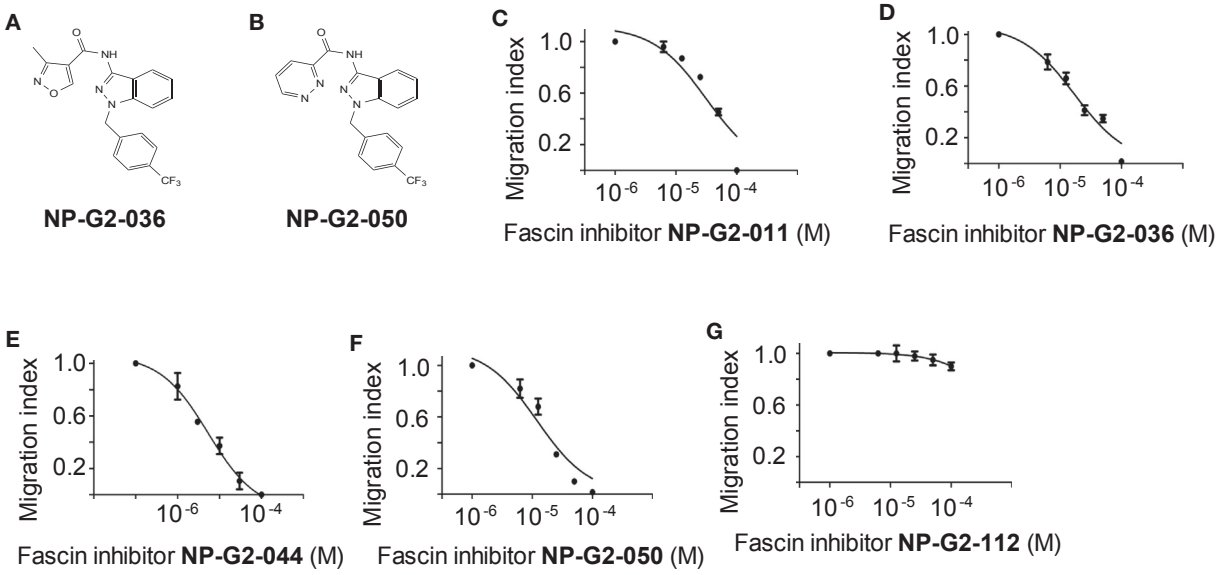

Figure 6 – Inhibitory effect of analogues of Compound G2 on breast tumor cell migration. (A) The chemical structure of Compound NP-G2-036. (B) The chemical structure of Compound NP-G2-050. (C) Inhibition of the migration of MDA-MB-231 cells by Compound NP-G2-011 in response to serum stimulation. (D) Inhibition of the migration of MDA-MB-231 cells by Compound NP-G2-036 in response to serum stimulation. (E) Inhibition of the migration of MDA-MB-231 cells by Compound NP-G2-044 in response to serum stimulation. (F) Inhibition of the migration of MDA-MB-231 cells by Compound NP-G2-050 in response to serum stimulation. (G) Migration of MDA-MB-231 cells in the presence of Compound NP-G2-112 in response to serum stimulation. Error bars, mean ± s.e.m.

The observation that **NP-G2-011** and **NP-G2-044** slightly decreased the growth of primary tumors at a later stage (after Day 21) was not expected. Previously we showed that siRNAs against fascin had no effect on the proliferation of breast tumor cells in tissue culture plates (Chen et al., 2010). The observed inhibition of these compounds on the growth of primary tumors in animal models might be due to the possible inhibition of breast tumor cell growth in three-dimensional environment or an inhibitory effect on tumor angiogenesis since endothelial cells express some levels of fascin proteins (Huang et al., 2015). A very recent modeling study suggests that tumor cell migration plays a key role in tumor growth in three-dimensional architecture by increasing cellular fitness without directly affecting tumor cell proliferation per se (Waclaw et al., 2015). If this is indeed the case, it would have significant impacts on future clinical trial designs for fascin inhibitors. The minor inhibitory effect on primary tumor growth at the late stages might also contribute to the observed decrease of tumor metastasis.

Our data uncover a role for fascin in lamellipodial formation. Although it has not been previously demonstrated that fascin is critical for lamellipodial formation, recent studies have demonstrated a close link between filopodia and lamellipodia. Despite their structural differences, these two cellular protrusions are much more closely related than previously anticipated. Filopodia have been suggested to serve as templates for the formation and orientation of lamellipodia in fibroblasts (Johnson et al., 2015; Nemethova et al., 2008). In neuronal growth cones, fascin was observed in filopodia and in the bundles that comprise the actin ribs throughout the lamellipodia (Cohan et al., 2001). It is possible that fascin is needed for the initial formation of actin bundles in lamellipodia (such as via the formation of filopodia) and then dissociates from actin filaments in mature lamellipodia. This might explain the localization of fascin mainly in mature filopodia and weakly in mature lamellipodia, and is consistent with the above hypothesis that filopodia could serve as templates for lamellipodial formation. Indeed, using high-resolution time-lapse imaging, we have demonstrated that filopodia could act as initiation hubs for new lamellipodia, and that inhibition of the actin-bundling activity of fascin decreases filopodial formation resulting in decreased lamellipodial formation.

Our data also reveal a role for the actin-bundling activity of fascin in stress fiber formation and focal adhesion turnover. When fascin-GFP fusion protein was expressed in cells, we noticed that fascin-GFP proteins could be seen on stress fibers. This was consistent with earlier reports that fascin was observed on stress fibers (Yamashiro-Matsumura and Matsumura, 1986). However, it was not clear whether fascin

independent ROIs from different cells for each condition) are shown along with the exponential fit (red line). (G) Corresponding recovery half-time obtained from FRAP analyses of GFP-FAK pre-treated with vehicle (Ctrl) or NP-G2-044. (H) Confocal live cell image of a representative MDA-MB-231 cell expressing GFP-FAK and a focal adhesion containing ROI (yellow box). (I) Kymograph of the corresponding focal adhesion over a period of 40 min. Acquisitions were taken every 30 s. (J) Quantitative assessment of focal adhesion disassembly in GFP-FAK expressing cells pre-treated with vehicle (Ctrl, blue square) or NP-G2-044 (red circle). (K) and (L) Assembly (K) and disassembly (L) rates were obtained by numerical differentiation of the corresponding time-dependent signal. Error bars, mean ± s.e.m. Scale bars, 10 μm *$p < 0.05$; **$p < 0.01$.

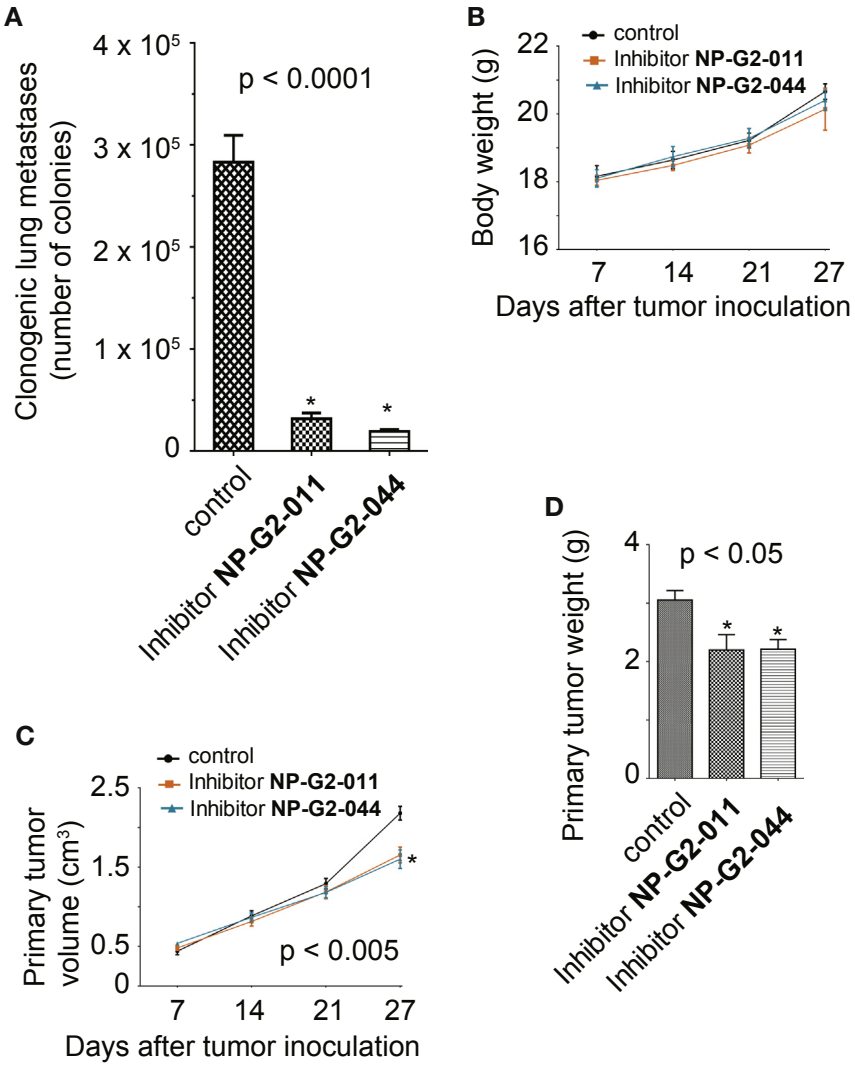

Figure 7 – Inhibitory effect of analogue NP-G2-011 and NP-G2-044 on breast tumor metastasis in mouse models. (A) Inhibition of 4T1 mouse mammary tumor cell metastasis to the lung by NP-G2-011 and NP-G2-044 in a spontaneous metastasis model (n = 5 for each group). (B) NP-G2-011 and NP-G2-044 had no effect on the body weights of treated mice. (C) NP-G2-011 and NP-G2-044 decreased the volume of primary tumors at later stages. (D) NP-G2-011 and NP-G2-044 decreased the primary tumor weight. Error bars, mean ± s.e.m.

is essential for the formation of stress fibers or simply localized on stress fibers. Recently it was reported that down-regulation of fascin protein levels by siRNAs in NIH 3T3 fibroblasts and in HCT116 colon cancer cells led to an ~20% increase of the thickness of actin stress fibers, but these thicker stress fibers appeared shorter than actin stress fibers in control siRNA-treated cells (Elkhatib et al., 2014). This is consistent with what we observed after treatment with **G2** analogues. Indeed, in our initial screening of small-molecule fascin inhibitors, we developed a high throughput screening method using fluorescent microscopy to visualize actin filament bundles and observed the main effect of fascin was to increase the length of actin filament bundles. Therefore, consistent with this in vitro observation, our cellular data show an inhibitory effect of fascin inhibitors on the formation of long actin stress fibers.

In summary, we have developed improved fascin-specific inhibitors. These inhibitors blocked tumor cell migration and metastasis. We have revealed the biochemical mechanism by which these inhibitors block the actin-bundling function of fascin. We have demonstrated that these inhibitors impaired actin cytoskeletal reorganization, thus providing potential cellular mechanisms by which these inhibitors block tumor cell migration. Given the clinical data pointing a role for fascin in tumor spreading in cancer patients, fascin inhibitors could be further developed for treating metastatic cancers.

Competing financial interests

Cornell University and Novita Pharmaceuticals filed a patent application on the fascin inhibitors described here. Novita Pharmaceuticals supported this work through a Sponsored Research Agreement. X.Y.H. and J.J.Z. are founders and have equity in Novita Pharmaceuticals. The remaining authors declare no competing financial interests.

Acknowledgments

We thank G. Wu and C. Shue for participation in the design and synthesis of chemical compounds and planning of this project; B. Ding and members of our laboratory for experimental advice and assistance. This work was supported by a Sponsored Research Agreement from Novita Pharmaceuticals to Weill Cornell Medical College.

REFERENCES

Adams, J.C., 2004. Roles of fascin in cell adhesion and motility. Curr. Opin. Cell Biol. 16, 590–596.

Aznavoorian, S., Murphy, A.N., Stetler-Stevenson, W.G., Liotta, L.A., 1993. Molecular aspects of tumor cell invasion and metastasis. Cancer 71, 1368–1383.

Bentley, D., Toroian-Raymond, A., 1986. Disoriented pathfinding by pioneer neurone growth cones deprived of filopodia by cytochalasin treatment. Nature 323, 712–715.

Bordeleau, F., Galarneau, L., Gilbert, S., Loranger, A., Marceau, N., 2010. Keratin 8/18 modulation of protein kinase C-mediated integrin-dependent adhesion and migration of liver epithelial cells. Mol. Biol. Cell 21, 1698–1713.

Bryan, J., Kane, R.E., 1978. Separation and interaction of the major components of sea urchin actin gel. J. Mol. Biol. 125, 207–224.

Cao, D., Ji, H., Ronnett, B.M., 2005. Expression of mesothelin, fascin, and prostate stem cell antigen in primary ovarian mucinous tumors and their utility in differentiating primary ovarian mucinous tumors from metastatic pancreatic mucinous carcinomas in the ovary. Int. J. Gynecol. Pathol. 24, 67–72.

Chen, L., Yang, S., Jakoncic, J., Zhang, J.J., Huang, X.Y., 2010. Migrastatin analogues target fascin to block tumour metastasis. Nature 464, 1062–1066.

Claessens, M.M., Bathe, M., Frey, E., Bausch, A.R., 2006. Actin-binding proteins sensitively mediate F-actin bundle stiffness. Nat. Mater. 5, 748–753.

Cohan, C.S., Welnhofer, E.A., Zhao, L., Matsumura, F., Yamashiro, S., 2001. Role of the actin bundling protein fascin in growth cone morphogenesis: localization in filopodia and lamellipodia. Cell Motil Cytoskeleton 48, 109–120.

Condeelis, J., Singer, R.H., Segall, J.E., 2005. The great escape: when cancer cells hijack the genes for chemotaxis and motility. Annu. Rev. Cell Dev. Biol. 21, 695–718.

Coopman, P.J., Do, M.T., Thompson, E.W., Mueller, S.C., 1998. Phagocytosis of cross-linked gelatin matrix by human breast carcinoma cells correlates with their invasive capacity. Clin. Cancer Res. 4, 507–515.

Darnel, A.D., Behmoaram, E., Vollmer, R.T., Corcos, J., Bijian, K., Sircar, K., Su, J., Jiao, J., Alaoui-Jamali, M.A., Bismar, T.A., 2009. Fascin regulates prostate cancer cell invasion and is associated with metastasis and biochemical failure in prostate cancer. Clin. Cancer Res. 15, 1376–1383.

Davenport, R.W., Dou, P., Rehder, V., Kater, S.B., 1993. A sensory role for neuronal growth cone filopodia. Nature 361, 721–724.

Davies, J.M., Goldberg, R.M., 2011. Treatment of metastatic colorectal cancer. Semin. Oncol. 38, 552–560.

Elkhatib, N., Neu, M.B., Zensen, C., Schmoller, K.M., Louvard, D., Bausch, A.R., Betz, T., Vignjevic, D.M., 2014. Fascin plays a role in stress fiber organization and focal adhesion disassembly. Curr. Biol. 24, 1492–1499.

Fidler, I.J., 2003. The pathogenesis of cancer metastasis: the 'seed and soil' hypothesis revisited. Nat. Rev. Cancer 3, 453–458.

Fornier, M.N., 2011. Approved agents for metastatic breast cancer. Semin. Oncol. 38 (Suppl. 2), S3–S10.

Grothey, A., Hashizume, R., Sahin, A.A., McCrea, P.D., 2000. Fascin, an actin-bundling protein associated with cell motility, is upregulated in hormone receptor negative breast cancer. Br. J. Cancer 83, 870–873.

Hamadi, A., Bouali, M., Dontenwill, M., Stoeckel, H., Takeda, K., Ronde, P., 2005. Regulation of focal adhesion dynamics and disassembly by phosphorylation of FAK at tyrosine 397. J. Cell Sci. 118, 4415–4425.

Hashimoto, Y., Kim, D.J., Adams, J.C., 2011. The roles of fascins in health and disease. J. Pathol. 224, 289–300.

Hashimoto, Y., Shimada, Y., Kawamura, J., Yamasaki, S., Imamura, M., 2004. The prognostic relevance of fascin expression in human gastric carcinoma. Oncology 67, 262–270.

Hashimoto, Y., Skacel, M., Adams, J.C., 2005. Roles of fascin in human carcinoma motility and signaling: prospects for a novel biomarker? Int. J. Biochem. Cel. Biol. 37, 1787–1804.

Huang, F.K., Han, S., Xing, B., Huang, J., Liu, B., Bordeleau, F., Reinhart-King, C.A., Zhang, J.J., Huang, X.Y., 2015. Targeted inhibition of fascin function blocks tumour invasion and metastatic colonization. Nat. Commun. 6, 7465.

Jaffe, A.B., Hall, A., 2005. Rho GTPases: biochemistry and biology. Annu. Rev. Cell Dev. Biol. 21, 247–269.

Jansen, S., Collins, A., Yang, C., Rebowski, G., Svitkina, T., Dominguez, R., 2011. Mechanism of actin filament bundling by fascin. J. Biol. Chem. 286, 30087–30096.

Johnson, H.E., King, S.J., Asokan, S.B., Rotty, J.D., Bear, J.E., Haugh, J.M., 2015. F-actin bundles direct the initiation and orientation of lamellipodia through adhesion-based signaling. J. Cell Biol. 208, 443–455.

Lee, L.Y., Chen, Y.J., Lu, Y.C., Liao, C.T., Chen, I.H., Chang, J.T., Huang, Y.C., Chen, W.H., Huang, C.C., Tsai, C.Y., Cheng, A.J., 2015. Fascin Is a Circulating Tumor Marker for Head and Neck cancer as Determined by a Proteomic Analysis of Interstitial Fluid from the Tumor Microenvironment. Clinical chemistry and laboratory medicine: CCLM/FESCC.

Li, A., Morton, J.P., Ma, Y., Karim, S.A., Zhou, Y., Faller, W.J., Woodham, E.F., Morris, H.T., Stevenson, R.P., Juin, A., et al., 2014. Fascin is regulated by slug, promotes progression of pancreatic cancer in mice, and is associated with patient outcomes. Gastroenterology 146, 1386–1396 e1381–1317.

Machesky, L.M., Li, A., 2010. Fascin: invasive filopodia promoting metastasis. Commun. Integr. Biol. 3, 263–270.

Maitra, A., Iacobuzio-Donahue, C., Rahman, A., Sohn, T.A., Argani, P., Meyer, R., Yeo, C.J., Cameron, J.L., Goggins, M., Kern, S.E., et al., 2002. Immunohistochemical validation of a novel epithelial and a novel stromal marker of pancreatic ductal adenocarcinoma identified by global expression microarrays: sea urchin fascin homolog and heat shock protein 47. Am. J. Clin. Pathol. 118, 52–59.

Mattila, P.K., Lappalainen, P., 2008. Filopodia: molecular architecture and cellular functions. Nat. Rev. Mol. Cell Biol. 9, 446–454.

Mogilner, A., Rubinstein, B., 2005. The physics of filopodial protrusion. Biophys. J. 89, 782–795.

Nemethova, M., Auinger, S., Small, J.V., 2008. Building the actin cytoskeleton: filopodia contribute to the construction of contractile bundles in the lamella. J. Cell Biol. 180, 1233–1244.

Otto, J.J., Kane, R.E., Bryan, J., 1979. Formation of filopodia in coelomocytes: localization of fascin, a 58,000 dalton actin cross-linking protein. Cell 17, 285–293.

Partin, A.W., Schoeniger, J.S., Mohler, J.L., Coffey, D.S., 1989. Fourier analysis of cell motility: correlation of motility with metastatic potential. Proc. Natl. Acad. Sci. U S A 86, 1254–1258.

Pelosi, G., Pasini, F., Fraggetta, F., Pastorino, U., Iannucci, A., Maisonneuve, P., Arrigoni, G., De Manzoni, G., Bresaola, E., Viale, G., 2003. Independent value of fascin immunoreactivity for predicting lymph node metastases in typical and atypical pulmonary carcinoids. Lung Cancer 42, 203–213.

Pulaski, B.A., Ostrand-Rosenberg, S., 1998. Reduction of established spontaneous mammary carcinoma metastases following immunotherapy with major histocompatibility complex class II and B7.1 cell-based tumor vaccines. Cancer Res. 58, 1486–1493.

Rodriguez-Pinilla, S.M., Sarrio, D., Honrado, E., Hardisson, D., Calero, F., Benitez, J., Palacios, J., 2006. Prognostic significance of basal-like phenotype and fascin expression in node-negative invasive breast carcinomas. Clin. Cancer Res. 12, 1533–1539.

Roussos, E.T., Condeelis, J.S., Patsialou, A., 2011. Chemotaxis in cancer. Nat. Rev. Cancer 11, 573–587.

Ruys, A.T., Groot Koerkamp, B., Wiggers, J.K., Klumpen, H.J., ten Kate, F.J., van Gulik, T.M., 2014. Prognostic biomarkers in patients with resected cholangiocarcinoma: a systematic review and meta-analysis. Ann. Surg. Oncol. 21, 487–500.

Sanders, T.A., Llagostera, E., Barna, M., 2013. Specialized filopodia direct long-range transport of SHH during vertebrate tissue patterning. Nature 497, 628–632.

Schoumacher, M., El-Marjou, F., Lae, M., Kambou, N., Louvard, D., Robine, S., Vignjevic, D.M., 2014. Conditional expression of fascin increases tumor progression in a mouse model of intestinal cancer. Eur. J. Cel. Biol. 93, 388–395.

Sedeh, R.S., Fedorov, A.A., Fedorov, E.V., Ono, S., Matsumura, F., Almo, S.C., Bathe, M., 2010. Structure, evolutionary conservation, and conformational dynamics of *Homo sapiens* fascin-1, an F-actin crosslinking protein. J. Mol. Biol. 400, 589–604.

Shan, D., Chen, L., Njardarson, J.T., Gaul, C., Ma, X., Danishefsky, S.J., Huang, X.Y., 2005. Synthetic analogues of migrastatin that inhibit mammary tumor metastasis in mice. Proc. Natl. Acad. Sci. U S A 102, 3772–3776.

Shibue, T., Brooks, M.W., Inan, M.F., Reinhardt, F., Weinberg, R.A., 2012. The outgrowth of micrometastases is enabled by the formation of filopodium-like protrusions. Cancer Discov. 2, 706–721.

Sondak, V.K., Han, D., Deneve, J., Kudchadkar, R., 2011. Current and planned multicenter trials for patients with primary or metastatic melanoma. J. Surg. Oncol. 104, 430–437.

Tan, V.Y., Lewis, S.J., Adams, J.C., Martin, R.M., 2013. Association of fascin-1 with mortality, disease progression and metastasis in carcinomas: a systematic review and meta-analysis. BMC Med. 11, 52.

Teng, Y., Xu, S., Yue, W., Ma, L., Zhang, L., Zhao, X., Guo, Y., Zhang, C., Gu, M., Wang, Y., 2013. Serological investigation of the clinical significance of fascin in non-small-cell lung cancer. Lung Cancer 82, 346–352.

Tilney, L.G., Connelly, P.S., Vranich, K.A., Shaw, M.K., Guild, G.M., 1998. Why are two different cross-linkers necessary for actin bundle formation in vivo and what does each cross-link contribute? J. Cell Biol. 143, 121–133.

Vignjevic, D., Kojima, S., Aratyn, Y., Danciu, O., Svitkina, T., Borisy, G.G., 2006. Role of fascin in filopodial protrusion. J. Cell Biol. 174, 863–875.

Vignjevic, D., Yarar, D., Welch, M.D., Peloquin, J., Svitkina, T., Borisy, G.G., 2003. Formation of filopodia-like bundles in vitro from a dendritic network. J. Cell Biol. 160, 951–962.

Waclaw, B., Bozic, I., Pittman, M.E., Hruban, R.H., Vogelstein, B., Nowak, M.A., 2015. A spatial model predicts that dispersal and cell turnover limit intratumour heterogeneity. Nature 525, 261–264.

Wang, W., Wyckoff, J.B., Frohlich, V.C., Oleynikov, Y., Huttelmaier, S., Zavadil, J., Cermak, L., Bottinger, E.P., Singer, R.H., White, J.G., et al., 2002. Single cell behavior in metastatic primary mammary tumors correlated with gene expression patterns revealed by molecular profiling. Cancer Res. 62, 6278–6288.

Yamakita, Y., Matsumura, F., Yamashiro, S., 2009. Fascin1 is dispensable for mouse development but is favorable for neonatal survival. Cell Motil Cytoskeleton 66, 524–534.

Yamashiro-Matsumura, S., Matsumura, F., 1985. Purification and characterization of an F-actin-bundling 55-kilodalton protein from HeLa cells. J. Biol. Chem. 260, 5087–5097.

Yamashiro-Matsumura, S., Matsumura, F., 1986. Intracellular localization of the 55-kD actin-bundling protein in cultured cells: spatial relationships with actin, alpha-actinin, tropomyosin, and fimbrin. J. Cell Biol. 103, 631–640.

Yang, S., Huang, F.K., Huang, J., Chen, S., Jakoncic, J., Leo-Macias, A., Diaz-Avalos, R., Chen, L., Zhang, J.J., Huang, X.Y., 2013. Molecular mechanism of fascin function in filopodial formation. J. Biol. Chem. 288, 274–284.

Yang, S., Zhang, J.J., Huang, X.Y., 2009. Orai1 and STIM1 are critical for breast tumor cell migration and metastasis. Cancer Cell 15, 124–134.

Yoder, B.J., Tso, E., Skacel, M., Pettay, J., Tarr, S., Budd, T., Tubbs, R.R., Adams, J.C., Hicks, D.G., 2005. The expression of fascin, an actin-bundling motility protein, correlates with hormone receptor-negative breast cancer and a more aggressive clinical course. Clin. Cancer Res. 11, 186–192.

Zigeuner, R., Droschl, N., Tauber, V., Rehak, P., Langner, C., 2006. Biologic significance of fascin expression in clear cell renal cell carcinoma: systematic analysis of primary and metastatic tumor tissues using a tissue microarray technique. Urology 68, 518–522.